# On the geometric misalignment in the design of helical CT with linear photon-counting detector arrays

Junho Lee <sup>a</sup>, Yoonsang Hong <sup>a</sup>, Junwoo Kim <sup>b</sup>, and Ho Kyung Kim <sup>a\*</sup>

<sup>a</sup>Computational X-ray Imaging Laboratory, School of Mechanical Engineering, Pusan National University,

Busandaehak-ro 63beon-gil, Geumjeong-gu, Busan 46241, Republic of Korea

<sup>b</sup>SAMSUNG Medison Co., Ltd., 1077, Cheonho-raero, Gangdong-gu, Seoul, 05340, Republic of Korea

\*Corresponding author: hokyung@pusan.kr

## \*Keywords: photon-counting detectors, geometric misalignment, geometric calibration, helical computed tomography

## 1. Introduction

In terms of operating principles, X-ray imaging detectors can be categorized energy-integrating detectors (EIDs) and photon-counting detectors (PCDs). The ability of PCDs to detect individual X-ray photons with precise energy discrimination offers significant advantages over conventional EIDs [1]. In addition, PCDs exhibit superior spatial resolution compared with EIDs, primarily due to smaller charge diffusion in semiconductors than light spreading in scintillators.

However, PCDs suffer from a limited field of view (FOV), mainly because of the restricted size of application-specific integrated circuits (ASICs). The FOV is further constrained by the limited dimensions of sensor materials, caused by electrical nonuniformity across crystal grains and the challenges of delicate bump-bonding/flip-chip technology for coupling sensors with ASICs as size increases. Although multiple PCD mosaics can be used to enlarge the FOV, implementing such configurations is technically demanding

While PCDs have been successfully adopted in computed tomography (CT), their application in large-area planer imaging, such as radiography and full-body CT, remains challenging, To mitigate this limitation, helical or spiral acquisition trajectories have been adopted in the medical field [2 Kishore2022, 3 Shikhjaliev2005].

In this work, we employ PCDs for helical CT and emphasize the necessity of geometric calibration, since even small mechanical misalignments can lead to severe geometric artifacts in reconstructed images. Following the framework of Zhang et al. [4], we will segment the helical acquisition path and acquire calibration phantom projections at multiple section points. The projection geometry parameters will then be determined using Noo's analytic method [5]. By interpolating the geometry along the helical trajectory, accurate system geometry can be estimated and subsequently applied to the helical reconstruction algorithm, thereby minimizing artifacts. This approach enables reliable large-volume imaging with PCDs, despite their limited detector size.

## 2. Methods and Materials

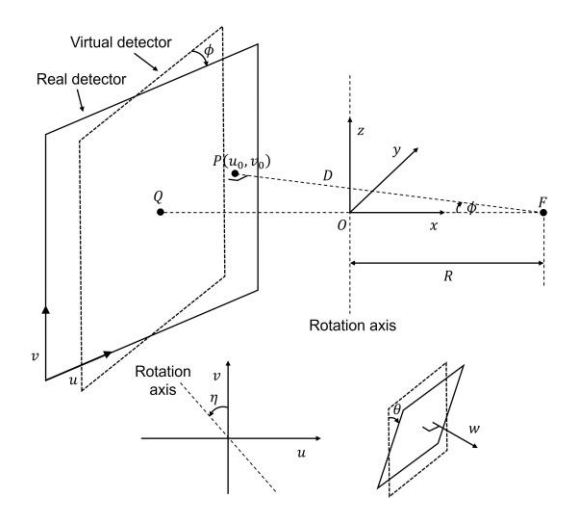


Fig. 1. Illustration of geometric misalignments in a CT system, including the X-ray source, rotation stage, and detector.

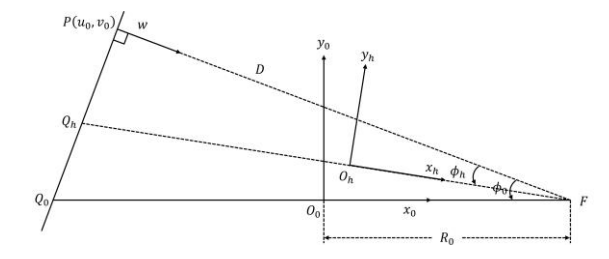


Fig. 2. Case of a helical CT system in which the translation axis is tilted relative to the rotation axis, leading to a shift in the effective origin  $O_b$  with height.

## 2.1 Geometric misalignment

In a CT system, geometric artifacts arise from misalignments among the X-ray source, the rotation stage, and the detector, as illustrated in Fig. 1. These misalignments can be described by the parameters D, R, P,  $\eta$ ,  $\phi$ , and  $\theta$ , which respectively represent: the shortest distance between the focal spot and the detector; the distance between the focal spot and the rotation stage; the coordinates of the orthogonal projection of the focal spot onto the detector plane; the angle between the detector's vertical axis (v) and the projection of the rotation axis; the angle between the rotation stage's y-axis and the

detector's horizontal axis (u); and the angle between the rotation stage's z-axis and the detector's vertical axis (v). These parameters can be estimated using a specially designed calibration phantom, typically consisting of precision-manufactured spheres (balls) arranged with known distances between them [5,6].

The calibration based on these parameters is valid in a general CT system. However, in a helical CT system, some parameters vary along the direction orthogonal to the rotation axis. Fig. 2 shows the case where the translation axis differs from the rotation axis (z-axis). Due to the tilt of the translation axis, the origin  $O_h$  changes as the stage translates; at each given height, the corresponding origin is denoted as  $O_h$ . Consequently, in a helical trajectory the parameters that depend on height are R and  $\phi$ , and the parameters at each specific height are defined  $R_h$  and  $\phi_h$ .

### 2.2 Parameter estimation

Using Noo's method, the parameters at a specific height can be estimated. Moreover, even if the position of the rotation axis changes, the vertical coordinate of  $Q_h$ , the intersection point between  $\overline{FO_h}$  and the detector plane, remains unchanged.

At a given vertical position  $T_i$ ,  $\phi_{T_i}$  can be calculated from the trajectory of a calibration sphere obtained through a circular scan, using Noo's method. Then, the horizontal detector coordinate  $u_{Q_{T_i}}$  of  $Q_{T_i}$  can be derived from the following equation:

$$u_{Q_{T_i}} = u_0 - D \tan \phi_{T_i}, \tag{1}$$

For an arbitrary vertical position  $h, u_{Q_h}$  can be estimated through linear interpolation as expressed below. Although  $u_{Q_h}$  is inherently a nonlinear function of h, if the spacing of T is chosen such that the interpolation error remains below one pixel, no artifacts appear in the calibration images [4].

$$u_{Q_h} = \frac{u_{Q_{T_{i+1}}} - u_{Q_{T_i}}}{T_i T_{i+1}} h + u_{Q_{T_i}}, \tag{2}$$

The corresponding  $\phi_h$  can then be computed from the following relation:

$$u_{Q_h} = u_{Q_{T_i}} - D \tan \phi_h, \tag{3}$$

As illustrated in Fig. 3, let the ascending direction vector of the motion stage be denoted as  $\vec{n}$ , with its components along the x, y, and z axes expressed as  $n_1$ ,  $n_2$ , and  $n_3$ , respectively:

$$n_1 = \sin \alpha \cos \beta, \tag{4}$$

$$n_2 = \sin \alpha \sin \beta, \tag{5}$$

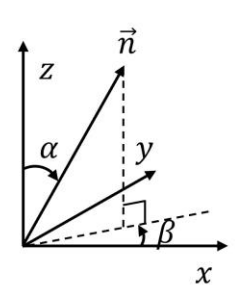


Fig. 3. Definition of the ascending direction vector  $\vec{n}$  of the motion stage and its components  $(n_1, n_2, n_3)$  along the x, y, and z axes.

$$n_3 = \cos \alpha, \tag{6}$$

The components of  $\vec{n}$  can then be derived using the following relations:

$$R_{T_{i+1}} = \sqrt{\left(R_{T_i} - n_1 \overline{T_i T_{i+1}}\right)^2 + (n_2 \overline{T_i T_{i+1}})^2},\tag{7}$$

$$R_{T_{i+1}}\cos(\phi_{T_i} - \phi_{T_{i+1}}) = R_{T_i} - n_1 \, \overline{T_i T_{i+1}},\tag{8}$$

Finally,  $R_h$  at an arbitrary height h can be calculated as:

$$R_h = \sqrt{\left(R_{T_i} - n_1 h\right)^2 + (n_2 h)^2},\tag{9}$$

## 2.3 Photon-counting detector

The PCD to be used in this study is a commercial XC-TDI200 (Direct Conversion AB, Sweden). The detector consists of eight small modules, each configured with  $64 \times 256$  pixels at a pitch of 0.1 mm, resulting in a total active field of view (FOV) of approximately  $6.4 \times 205$  mm ( $64 \times 2048$  pixels). The sensor material is cadmium telluride with a thickness of 2 mm, optimized for X-ray detection in the diagnostic and industrial energy ranges.

The PCD is equipped with an anti-coincidence (AC) option, which mitigates charge-sharing artifacts by reallocating charges dispersed across neighboring pixels to the pixel with the highest collected charge. With the AC option enabled, the detector provides improved reliability in X-ray photon counting, although the maximum count rate becomes limited. Without the AC option, charge sharing can introduce distortions, but the count rate capability extends up to  $5 \times 10^8 \ \text{mm}^{-2} \cdot \text{s}^{-1}$ , as specified by the manufacturer.

Although this PCD has not yet been applied to helical CT calibration experiments, the planned experiments will explore its potential for accurate geometric calibration in large-volume imaging despite its limited active area.

## 3. Preliminary Results

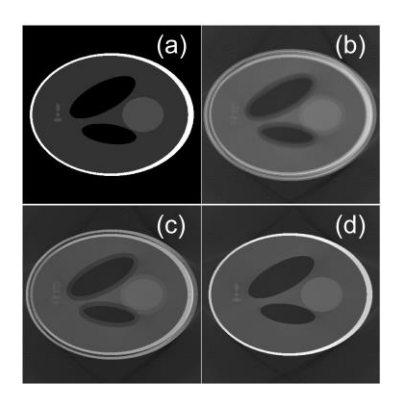


Fig. 4. Simulation results demonstrating the occurrence and suppression of misalignment artifacts in helical CT reconstruction. (a) 3D Shepp–Logan phantom used in the simulation. (b) Axial slice at  $z=100\,\mathrm{mm}$  without calibration, showing strong misalignment artifacts. (c) Reconstruction using parameters estimated only at  $z=0\,\mathrm{mm}$ , reducing but not eliminating artifacts. (d) Reconstruction with height-dependent calibration via interpolation, effectively removing misalignment artifacts.

Fig. 4 illustrates representative artifacts that can arise during helical CT reconstruction and their suppression depending on the applied calibration strategy.

Fig. 4(a) shows the 3D Shepp-Logan phantom used in the simulation, with physical dimensions of 10, 10, and 60 mm along the x, y, and z axes, respectively. A total helical scan was performed over a length of 200 mm, with the source-to-detector distance set to 1400 mm, The initial geometric parameters were chosen as  $R_0 = 150$  mm,  $\eta = 1^{\circ}$ ,  $\theta = 0^{\circ}$ ,  $\phi_0 = 1^{\circ}$ , and tilt angles  $\alpha = 2^{\circ}$ ,  $\beta = 2^{\circ}$ . Reconstruction was performed using the Feldkamp-Davis-Kress (FDK) algorithm in all cases.

Fig. 4(b) presents a reconstructed axial slice at z = 100 mm without any calibration. Strong geometric misalignment artifacts are clearly visible, including double-edge contours that degrade image quality.

Fig. 4(c) shows a reconstruction in which calibration parameters estimated at z=0 mm using Noo's method were applied. Compared with Fig. 4(b), the misalignment artifacts are reduced, although residual artifacts remain due to the height-dependent variation of system geometry in helical scanning.

Finally, Fig. 4(d) demonstrates a reconstruction of where parameters were estimated every 50 mm along the vertical direction (from z=0 to z=200 mm) and interpolated across the helical trajectory. In this case, the misalignment artifacts are effectively eliminated, yielding a visually clean reconstruction. This result emphasizes the necessity of height-dependent calibration in helical CT to ensure geometric artifacts-free volumetric imaging.

## 4. Conclusion and Future study

In this work, we investigated the impact of geometric misalignment in helical CT systems. Through simulation studies, we confirmed that even small deviations in system geometry can introduce severe misalignment artifacts in reconstructed images. We demonstrated that applying calibration parameters obtained from a single axial plane reduces artifacts to some extent, but residual distortions remain due to height-dependent variations in system geometry. By interpolating calibration parameters across multiple vertical positions, artifacts were effectively eliminated, highlighting the necessity of height-dependent calibration for reliable volumetric reconstruction in helical CT.

Future work will focus on experimental validation using a commercial PCD. Although calibration experiments with PCDs have not yet been performed, we plan to implement the proposed calibration framework in a real helical CT system. This will allow us to assess the robustness of the interpolation-based calibration strategy under realistic imaging conditions, and to evaluate the potential of PCDs for high-resolution, artifact-free large-volume imaging.

### **ACKNOWLEDGEMENTS**

This work was supported by the National Research Foundation of Korea (NRF) grant funded by the Korea government (MSIT) (RS-2024-00340520).

## REFERENCES

- [1] M. Danielsson, M. Persson, and M. Sjölin, Photon-counting x-ray detectors for CT, *Phys. Med. Biol.*, Vol. 66, No. 3, p. 03TR01, 2021.
- [2] K. Rajendran *et al.*, First clinical photon-counting detector CT system: technical evaluation, *Radiology*, Vol. 303, No. 1, pp. 130–138, 2022.
- [3] P. M. Shikhaliev, T. Xu, and S. Molloi, Photon counting computed tomography: concept and initial results, *Medical Physics*, Vol. 32, No. 2, pp. 427–436, 2005.
- [4] F. Zhang, B. Yan, L. Li, X. Xi, and H. Jiang, Practical geometric calibration for helical cone-beam industrial computed tomography, *Journal of X-ray Science and Technology*, Vol. 22, No. 1, pp. 19–35, 2014.
- [5] F. Noo, R. Clackdoyle, C. Mennessier, T. A. White, and T. J. Roney, Analytic method based on identification of ellipse parameters for scanner calibration in cone-beam tomography, *Physics in Medicine & Biology*, Vol. 45, No. 11, p. 3489, 2000. [6] K. Yang, A. L. C. Kwan, D. F. Miller, and J. M. Boone, A geometric calibration method for cone beam CT systems, *Medical Physics*, Vol. 33, No. 6, pp. 1695–1706, 2006.